

Aircraft Observations for Improved Physical Parameterization for Seasonal Prediction

Djamal Khelif

Department of Mechanical and Aerospace Engineering

University of California, Irvine

Irvine, CA 92697-3975

phone: (949) 824-7437 fax: (949) 824-8585 email: dkhelif@uci.edu

Award Number: N00014-12-1-0444

LONG-TERM GOALS

The long-term goals of our research are to understand and parameterize the physics of air-sea interaction and the Marine Atmospheric Boundary Layer (MABL) over a wide spectrum of wind speeds, sea state and cloud coverage.

OBJECTIVES

The objective of this effort is to obtain extensive measurements in the MABL under different cloud fractions specially aimed at quantifying various statistical quantities needed to examine and develop PDF-based cloud and turbulence parameterizations. The data set produced will help us understand the characteristics of empirical PDF of various dynamic and thermodynamic variables and their relevant turbulent statistics. In particular, we seek to understand the interplay among various physical processes in the cloudy boundary layer including surface forcing, longwave radiative cooling and shortwave radiative warming, turbulence transport, cloud microphysics, and entrainment and relate these processes to the PDF analyses. These measurements and analyses will be used by our collaborating modelers to evaluate different PDF cloud parameterization schemes in meso- and large scale forecast models with the goal of developing new parameterizations.

APPROACH

To achieve these objectives, we participated in the Unified Physical Parameterization for Extended Forecast (UPPEF) experiment and conducted aircraft measurements in the MABL off Monterey Bay under various cloud fraction conditions in the summer of 2012. We used the CIRPAS Twin Otter (TO) research aircraft that we instrumented with proven turbulence instrumentation for previous ONR projects to measure mean and turbulent wind components, temperature and humidity and associated air-sea fluxes. Specifically for this study, we made improvements to the instruments especially for humidity with the use of the fast-response UCI-modified LI-7200 enclosed path and the LI-7500 and the open-path H₂O/CO₂ analyzers in addition to our modified fast-response Krypton hygrometer. The radome wind gust sensing system was also completely overhauled. The main instrumentation on the TO is shown on Fig. 1. Similar measurements were also made with the Controlled Towed Vehicle (CTV). This is a modified target drone that we have been developing for air-sea interaction measurements and equipped with instruments to that of the TO. The CTV is towed by the TO via a thin

steel cable and is capable of active height-keeping as low as 10 m above sea level and 300 m below the TO.

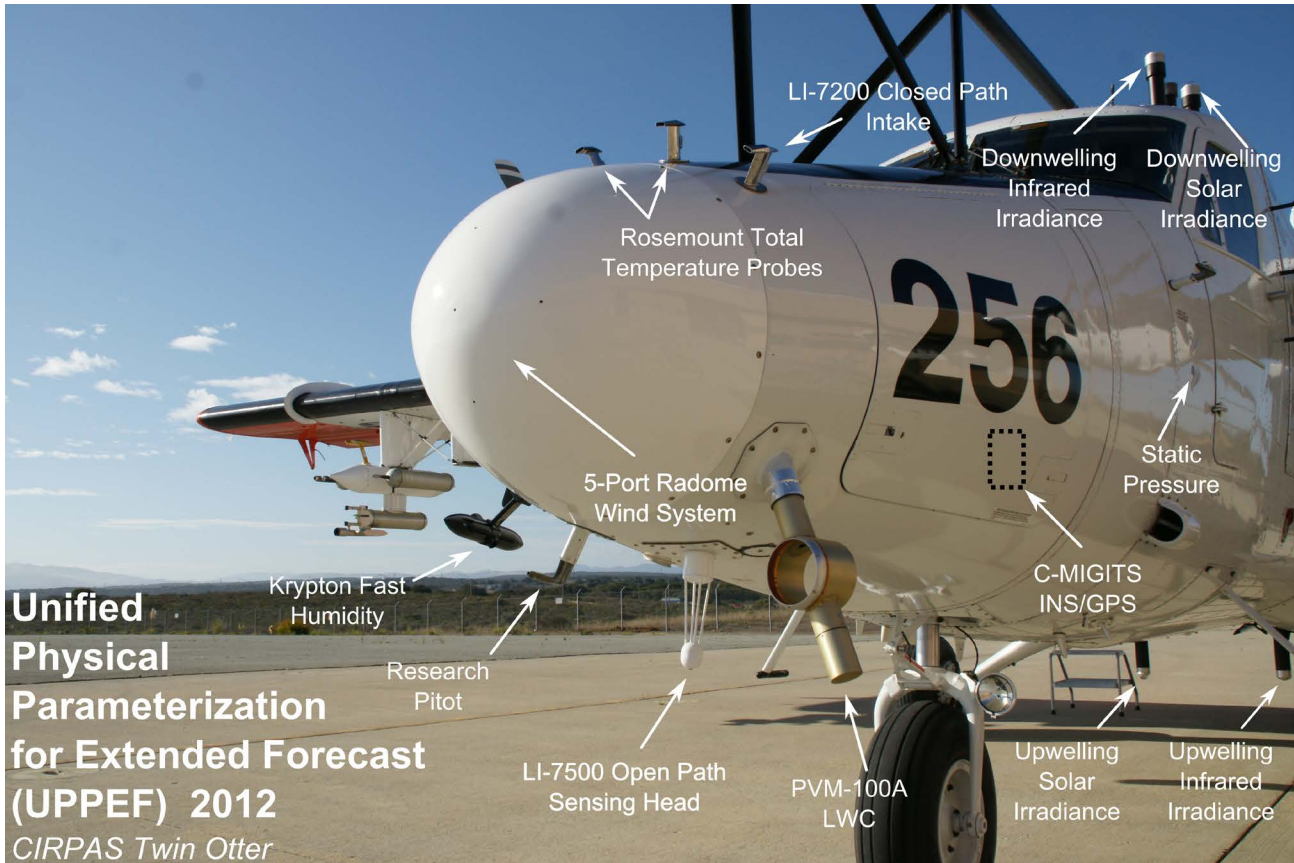


Figure 1. Turbulence and meteorological instrumentation installed on the CIRPAS Twin Otter aircraft for UPPEF 2012.

The TO flew a total of 12 UPPEF flights (and one overland wind lidar flight) depending on the cloud cover condition and the objectives of each given flight several track patterns varying from “L”, “U”, “S”, box, and long linear outbound/inbound transects were flown as shown in Fig. 2. The 3-D flight track with contours of potential temperature, θ , and dewpoint temperature T_d for the long linear outbound/inbound transects pattern on September 19, 2013 are also shown in Fig. 2. It shows that boundary layer height (identified with abrupt change θ and in T_d at the inversion) steadily increased with offshore distance.

WORK COMPLETED

High quality turbulence and meteorological measurements were obtained from the 12 UPPEF flights. The data were processed immediately after completion of each flight for quick-look and analysis. More rigorous processing and data quality control was systematically performed on data from all instruments we contributed and on data from instruments from other PIs (like the radiation package) that are

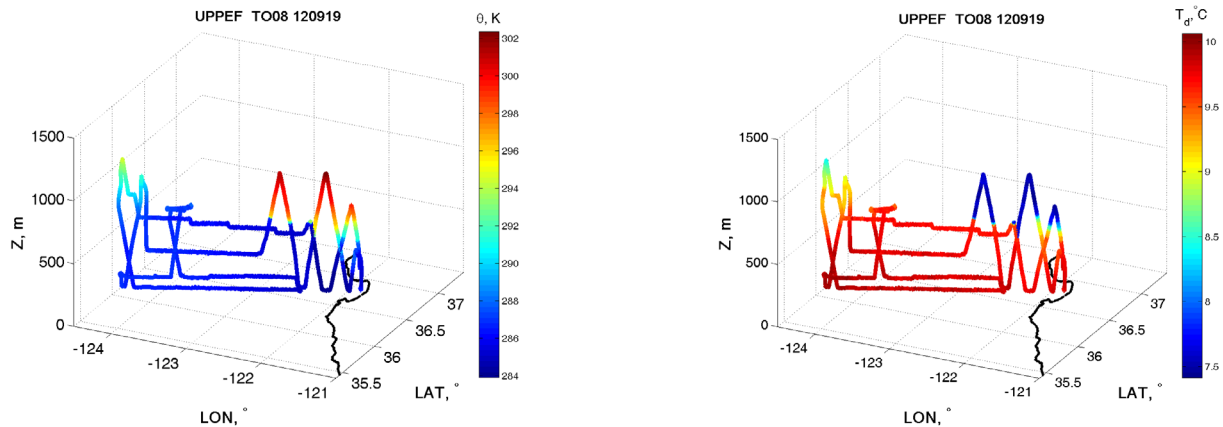
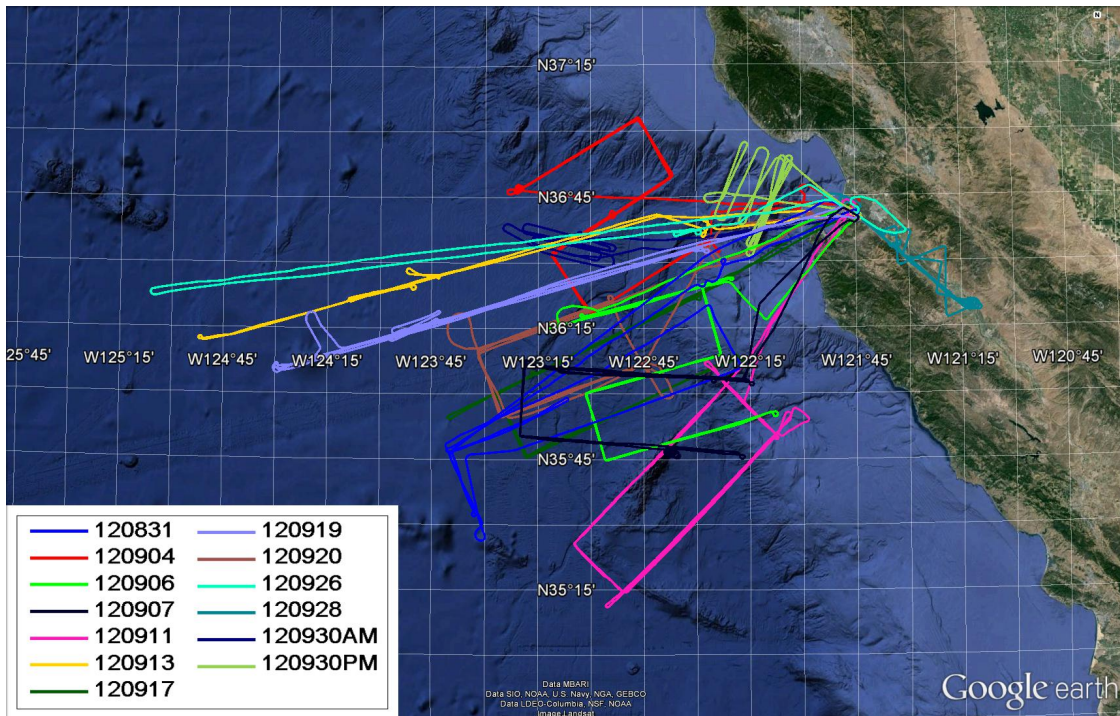


Figure 2. Twin Otter 2-D flight tracks during UPPEF where each flight is identified by its YYMMDD UTC date in the legend (top); 3-D track on the long outbound transect and back on September 19, 2012 with contours of potential temperature, θ , (bottom, left) and dew point temperature T_d (bottom, right). Note the increase of boundary layer height (identified with abrupt change θ and in T_d at the inversion) with offshore distance.

required for our research effort. Overall, the instruments performed very well as summarized in Table 1. There were two main data system on the aircraft: CIRPAS's and UCI's. Data from the TO instruments listed in this table were either recorded on the UCI data system (blue background) or CIRPAS's (yellow background) or on both (purple background) for redundancy. There was also a redundancy in many of the sensing systems to ensure that no data are lost due to instrument

malfunction. A good example of this is the humidity that was measured by 3 UCI's fast-response instruments and CIRPAS's reference chilled mirror slow-response dewpointer. Water vapor density (absolute humidity) data from these 4 sensors are shown in Fig. 3 for September 07, 2013 flight. The UCI modified krypton KH2O and the open path LI-7500 ranges were deliberately set for higher humidity values typical of those encountered near the ocean surface which explains why their signals are "clipped" at lower humidity values. The detailed plot of the up and down soundings through the inversion on the lower panel of Fig. 3 illustrates the lag in the chilled mirror response as well as an artificial oscillation on its signal due the Peltier thermoelectric mirror cooling having a hard time adjusting to fast transition from very dry to moist air during the descent soundings.

Table 1. Aircraft instrumentation performance summary during UPPEF experiment in 2012. Data from instruments with blue and light purple background are logged on UCI data system. Note that TO11 (09/28/2012) was an overland flight dedicated to Dave Emmitt's wind lidar.

		Unified Physical Parameterization for Extended Forecast (UPPEF) Aug-Sep 2012														
		UTC Day		08/31	09/04	09/06	09/07	09/11	09/13	09/17	09/19	09/20	09/26	09/28	09/30	09/30
		Instrument / Parameter		TO1	TO2	TO3	TO4	TO5	TO6	TO7	TO8	TO9	TO10	TO11 xx	TO12	TO13
Contact Scientist		dkhelif@uci.edu														
		hjonsson@nps.edu														
Temp		Rosemount Temperature (UCI)														
		Rosemount Temperature (CIRPAS)														
Humidity		Fast LI-COR 7200 Humidity (UCI)														
		Fast LI-COR 7500 Humidity (UCI)														
		Fast Mod. Krypton Hygrometer (UCI)														
		Edge-Tech Vigilent Dewpoint (CIRPAS)													xxx	xxx
CO2		Fast LI-COR 7500 CO2 (UCI)														
		Fast LI-COR 7200 CO2 (UCI)														
Alt		Roke MRA II Radar Altimeter (UCI)														
		Radar Altimeter (CIRPAS)														
Winds		Static Pressure (CIRPAS)														
		Radome Gust System (UCI) (x)														
INS / GPS		C-MIGITS (UCI)														
		OXTS RT3003 (UCI)														
		OXTS Base Station (UCI)														
		C-MIGITS (CIRPAS)														
		Novatel (CIRPAS)														
Radiation		TansVector(CIRPAS)														
		IR SST KT19 (CIRPAS)														
		Upward-looking IR Temperature KT19 (UCI)														
		Upwelling SW Radiometer (NRL / CIRPAS)														
		Upwelling LW Radiometer (NRL / CIRPAS)														
		Downwelling SW Radiometer (NRL / CIRPAS)														
Clouds / Aerosols		Downwelling LW Radiometer (NRL / CIRPAS)														
		TSI 3025 UFCPC (CIRPAS)														
		PCASP (CIRPAS)														
		FSSP-100 (CIRPAS)														
		CAPS (CIRPAS)														
		PVM-100A LWC														
		DMT-CCN (CIRPAS)														
		Controlled Towed Vehicle (CTV) (UCI)														
	TODWL (Simpson Weather Associates)															

Data System	UCI	CIRPAS and UCI	CIRPAS	SWA		
Instruments Status	Operational	Oscillations	Some Data	No data	Removed	QC Needed
Footnotes	(x) Different processing		(xx) Over Land		(xxx) Clipped	

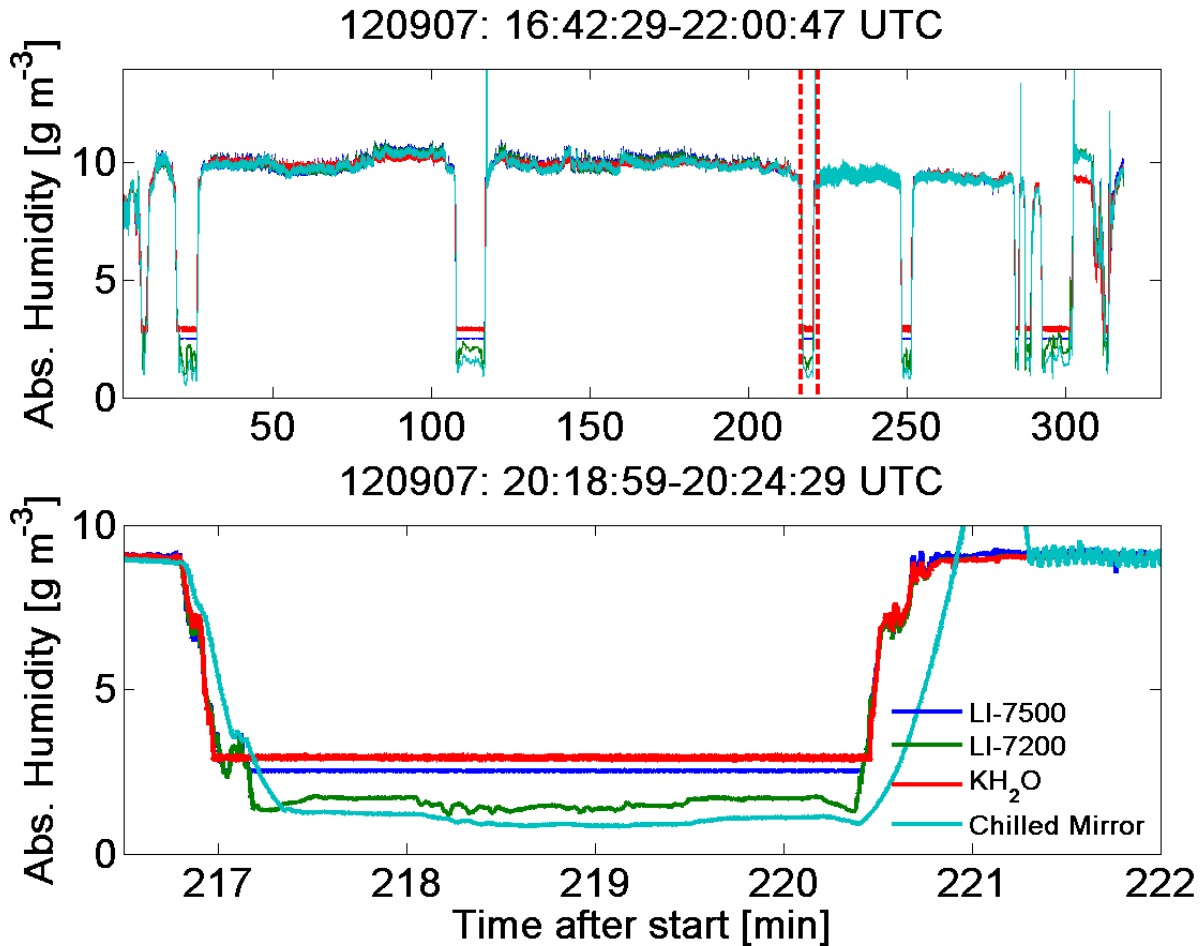


Figure 3. Absolute humidity from UCI fast-response sensors LI-7500 (blue), LI-7200 (green), krypton KH₂O (red) and CIRPAS slow-response chilled mirror (cyan). Data are from most of September 07, 2012 flight (top panel) and from the section delineated by red dotted vertical lines (bottom panel).

So far 3 processing iterations were performed on data from all flights. The UCI 40-Hz data set and its descriptive “header” file are available on our data server.

RESULTS

Preliminary analysis of the data was performed and we present in this section sample results from the TO measurements and then results from the CTV and discussion of the significant improvements we made to this platform in the past year. Data from each TO flight were first separated into soundings legs and straight and level runs. Eddy correlation fluxes and mean variables were calculated from 3-minutes (corresponding to ~10 km) contiguous segments that were “cut” on all level and straight runs. The ogive method was used to determine the flux estimates as the asymptote value towards the low-frequencies on the cumulative integral (integration done from high to low frequencies) of the cross-spectrum between the wind vertical component and the relevant variable. Results from 211 lowest

levels (~ 45 m or less) segments are shown on Fig. 4 (means) and Fig. 5 (fluxes) for all UPPEF flights except for the September 28, 2012 flight which was dedicated for the Simpson Associates wind lidar measurements overland. Each green dot on these plots represents data from one 10-km segment and the blue line represents the averages from all segments on the given flight. In general, the variability and trend of the fluxes reflect those of the means of the variables they are associated with.

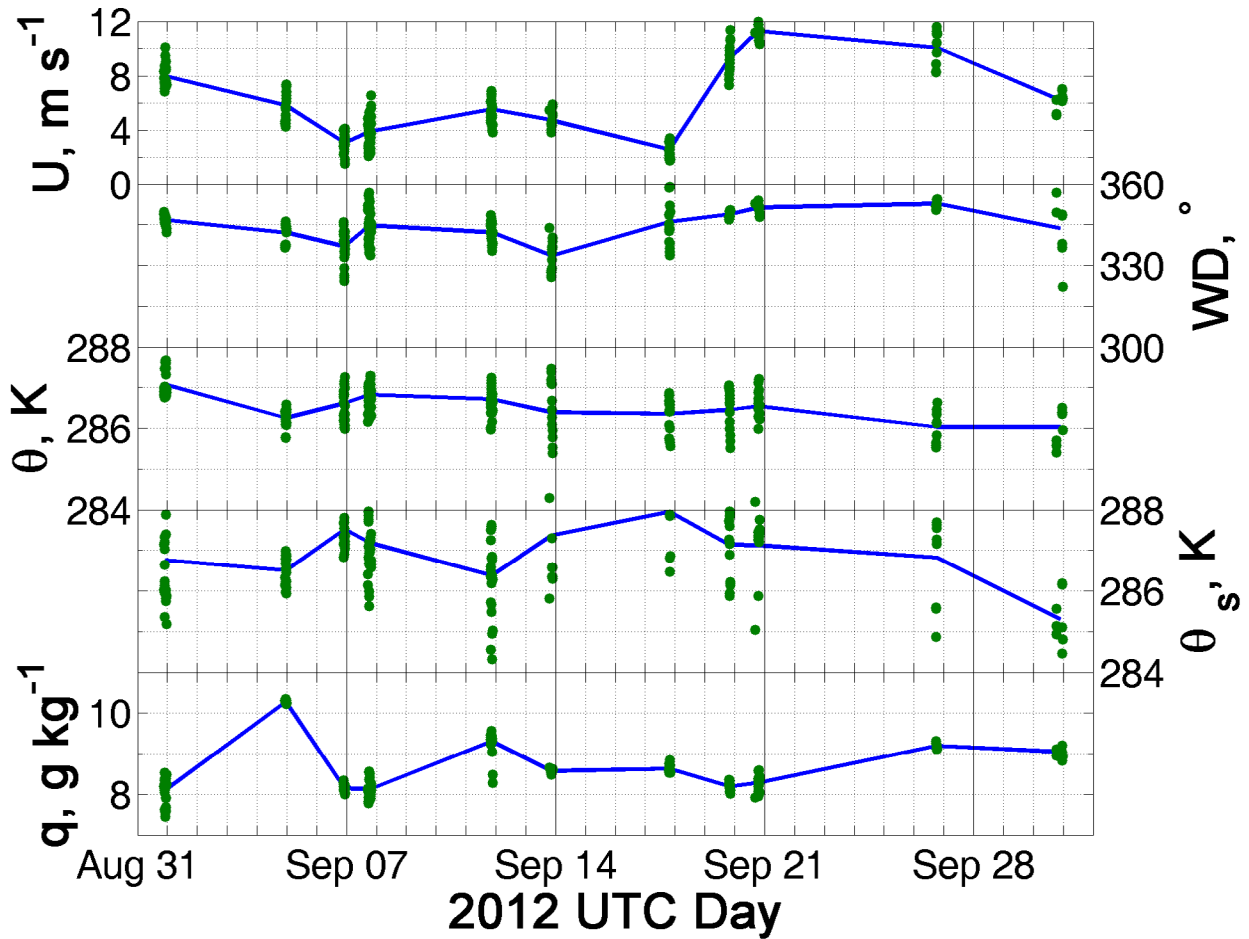


Figure 4. Mean variables obtained from 211 3-minute (~ 10 km) segments from straight and level runs at $z \leq 45$ m. Each green dot represents the average from one such segment and the blue line the flight average of (from to bottom) wind speed, wind direction, air potential temperature, radiometric sea surface temperature and specific humidity.

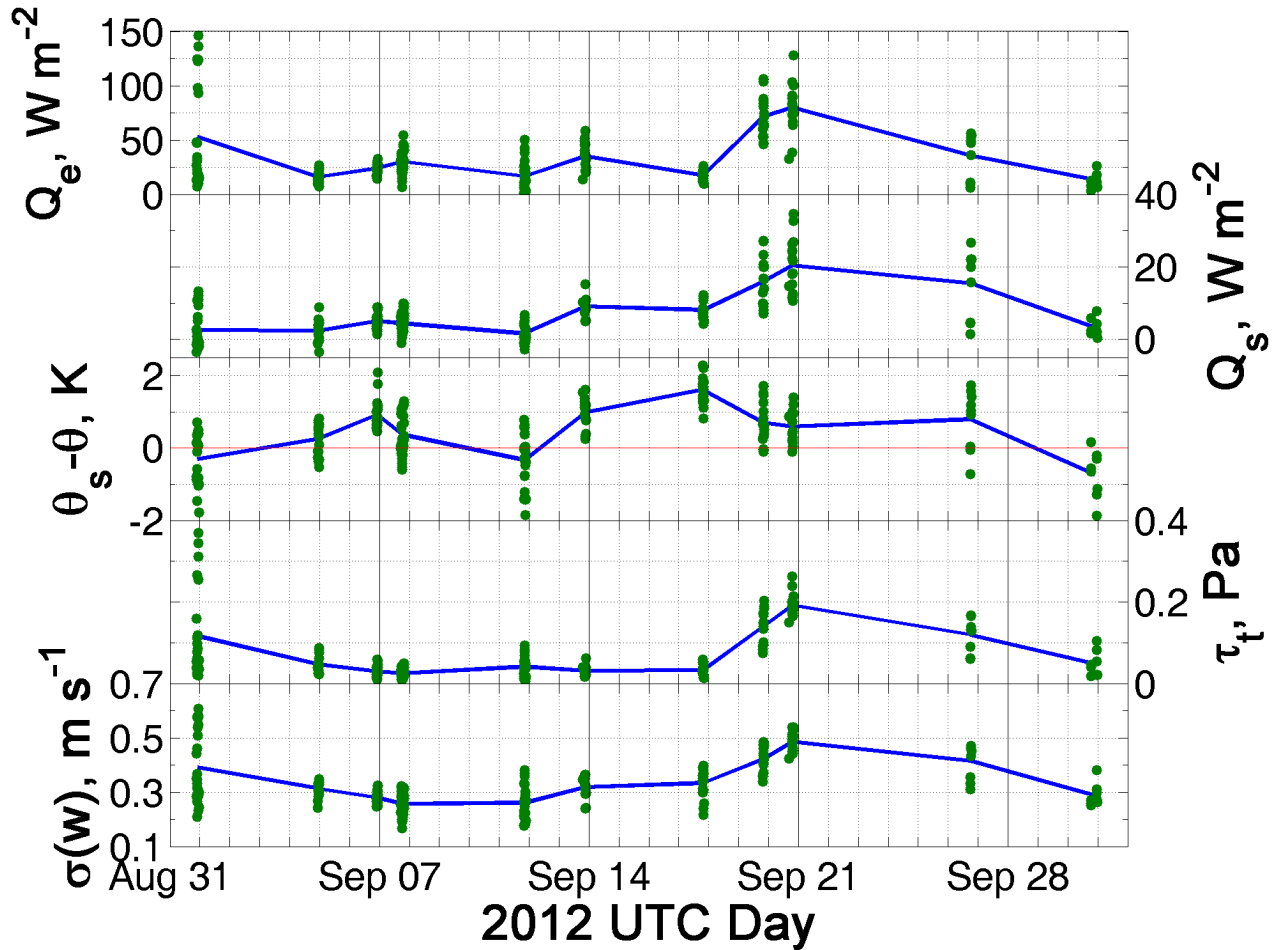


Figure 5. Eddy correlation fluxes obtained from 211 3-minute (~ 10 km) segments from straight and level runs at $z \leq 45$ m. Each green dot represents the estimate from one such segment and the blue line the flight average of (from top to bottom), latent heat flux, sensible heat flux, sea surface-air potential temperatures difference, stress and standard deviation of the wind vertical component.

While expected natural variability due to spatial inhomogeneities of the mean quantities and fluxes within each flight is observed on most flights, the variability of the fluxes on the first UPPEF flight (August 31, 2013) stands out. This is due to a very strong (3°C) SST front that was present on that day (Fig. 6). The originally planned “L” flight pattern had to be altered on-the-fly after the SST front was detected and straight and level runs at 33 m and at 95 m across the SST front were flown. From these runs, time series of turbulent fluxes were calculated using the running averaging technique with a 180-s (~ 10 km) sliding window. Results showing the air-sea interaction response to the SST front are shown in Fig. 7. A dramatic enhancement of turbulence intensity and turbulent fluxes is observed on the high temperature side of the SST front. On the 33-m TO run, the sensible heat flux increased from ~ 0 to $\sim 14 \text{ W m}^{-2}$, the latent heat flux increased from 10 to $\sim 160 \text{ W m}^{-2}$ and the total stress increased from ~ 0.02 to 0.40 Pa . The standard deviations of the vertical wind speed, horizontal wind speed and water vapor density jumped from 0.24 to 0.60 m s^{-1} , 0.43 to 1.00 m s^{-1} and 0.10 to 0.27 g m^{-3} , respectively, when moving from the cool side to the warm side of the SST front. The very large increase in latent heat flux is due to dryer air over the warm SST side and the presence of structures of different scales in the humidity signal. Similar observation can be made for the data from the 95-m run.

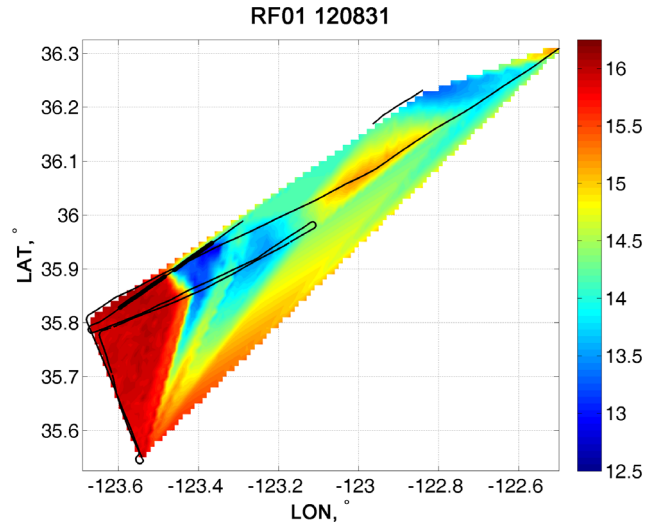


Figure 6. SST contour obtained from the Twin Otter IR pyrometer measurements on August 31, 2012 flight. The track of the aircraft legs at ~ 33 m and ~ 95 m are shown with a thin black line. The two thicker black lines are the two segments of the 33-m leg from which statistics on cool and warm sides of the SST front are given the text.

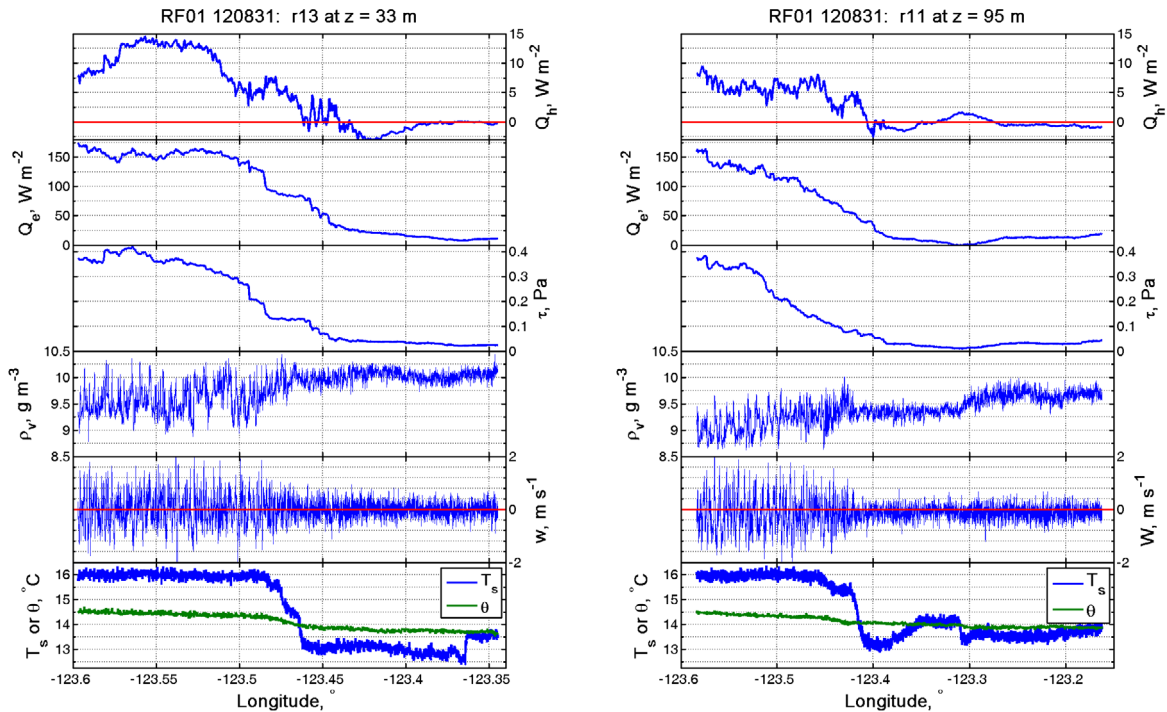


Figure 7. Variations of (from top to bottom) sensible heat flux, latent heat flux, total stress, vertical component of wind, water vapor density, radiometric sea surface temperature and air potential temperature on reciprocal 33-m (left) and ~ 95 -m (right) Twin Otter runs across a strong (~ 3 °C) SST front on August 31, 2012. A running averaging technique with a sliding window of 180 s (~ 10 km) was used for the eddy correlation flux estimates.

Plots showing variations (as a function of with wind speed) of the friction velocity squared, u^{*2} , and the drag coefficient, C_D , obtained from eddy correlation estimate of the stress on 180-s (~ 10 km) segments at ~ 33 m from all 12 UPPEF flights are presented in Fig. 8 below. For low winds (< 5 m s^{-1}) u^{*2} varies little with wind speed while C_D shows large scatter. Above 5 m s^{-1} or so, u^{*2} , increases with wind speed and C_D displays less scatter. The u^{*2} outliers around ~ 8.5 -9 m s^{-1} correspond to the enhanced fluxes on the warm side of the SST front.

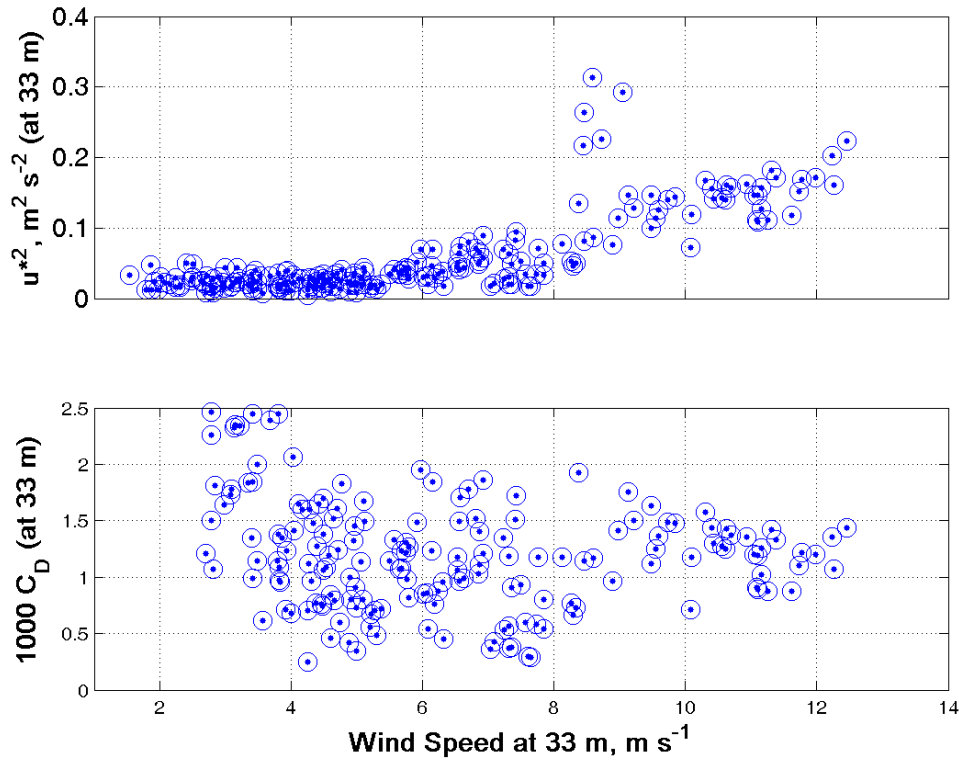


Figure 8. Variations of the squared friction velocity with (top) and drag coefficient $\times 1000$ (bottom) with mean wind speed at flight level at ~ 33 m.

We explored the variability of the latent heat flux and sensible heat flux over a long (~ 110 km) run flown at 35 m on 31 Aug 2012. Time series of these fluxes were obtained using a running averaging technique on the instantaneous products $w'\theta'$ and $w'\rho_v'$ using a 180-s (~ 10 km) sliding window. These fluxes are shown on the top panels of Fig. 9 with associated instantaneous meteorological variables. The latent heat flux seems to reflect (anti-correlated) variations in the observed water vapor density while the sensible heat flux is correlated with its driving sea-air temperature difference. The end of the long track is dominated by the sudden increase of air-sea interaction due to the crossing to the warm side of the strong SST front. Ogives of the two fluxes from this same run were estimated over 180-s contiguous segments “cut” on the long run and are shown in Fig. 10. The asymptote value of each curve toward the low frequencies end represents one estimate of the corresponding eddy covariance flux. It can be clearly seen that these values vary over a wide range as a result of the horizontal heterogeneities being sampled along the flight path. It can also be observed that the eddies that contribute the most to the flux range roughly from 55 m to 1300 m in size.

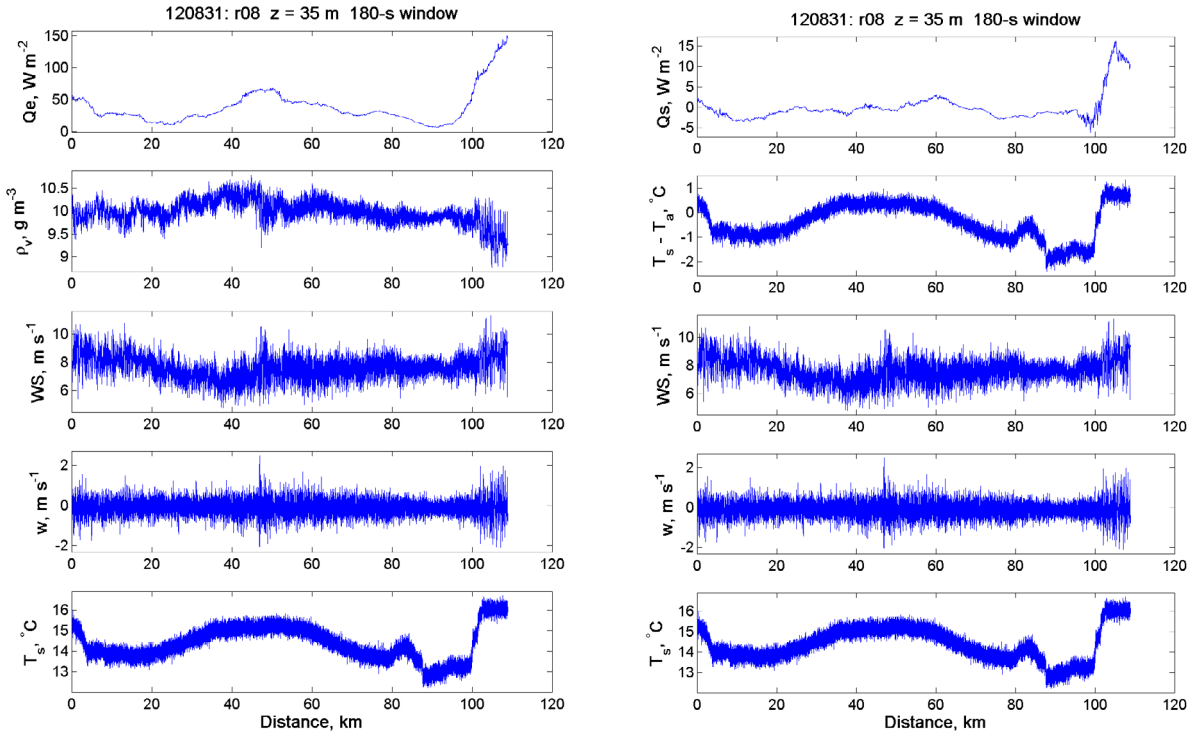


Figure 9. Latent heat (left, top) and sensible heat (right, top) fluxes variability over a long run (~110 km) at 35 m. Also shown (from bottom to top), radiometric sea surface temperature, wind vertical component, wind speed, water vapor density (left) and sea surface – ambient air temperature difference (right).

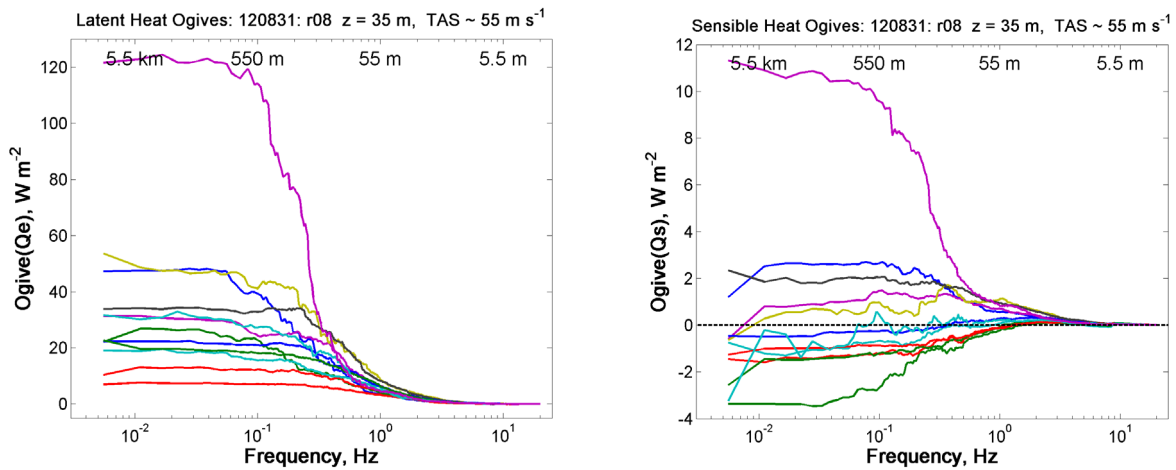


Figure 10. Latent heat (left) and sensible heat (right) fluxes ogives estimated over 180-s contiguous segments “cut” on the long run shown in Fig. 9. The asymptote value of each curve toward the low frequencies represents one estimate of the eddy covariance flux. Distances based on the aircraft mean true airspeed of 55 m s^{-1} are given at top of each panel to show the eddy scales that contribute most to the flux (~55 to 1300 m).

A recent addition to the Twin Otter is the Controlled Towed Vehicle (CTV) shown on Fig. 11. It is a modified target drone that we instrumented for the same turbulence measurements as on the Twin Otter itself. It has been demonstrated to maintain radar altitude height of 10 m above ocean waves while towed from the Twin Otter safely flying 305 m above. The main advantage of the CTV is the direct measurement of mean variables, turbulence and associated eddy covariance fluxes at the canonical air-sea interaction height of 10 m.

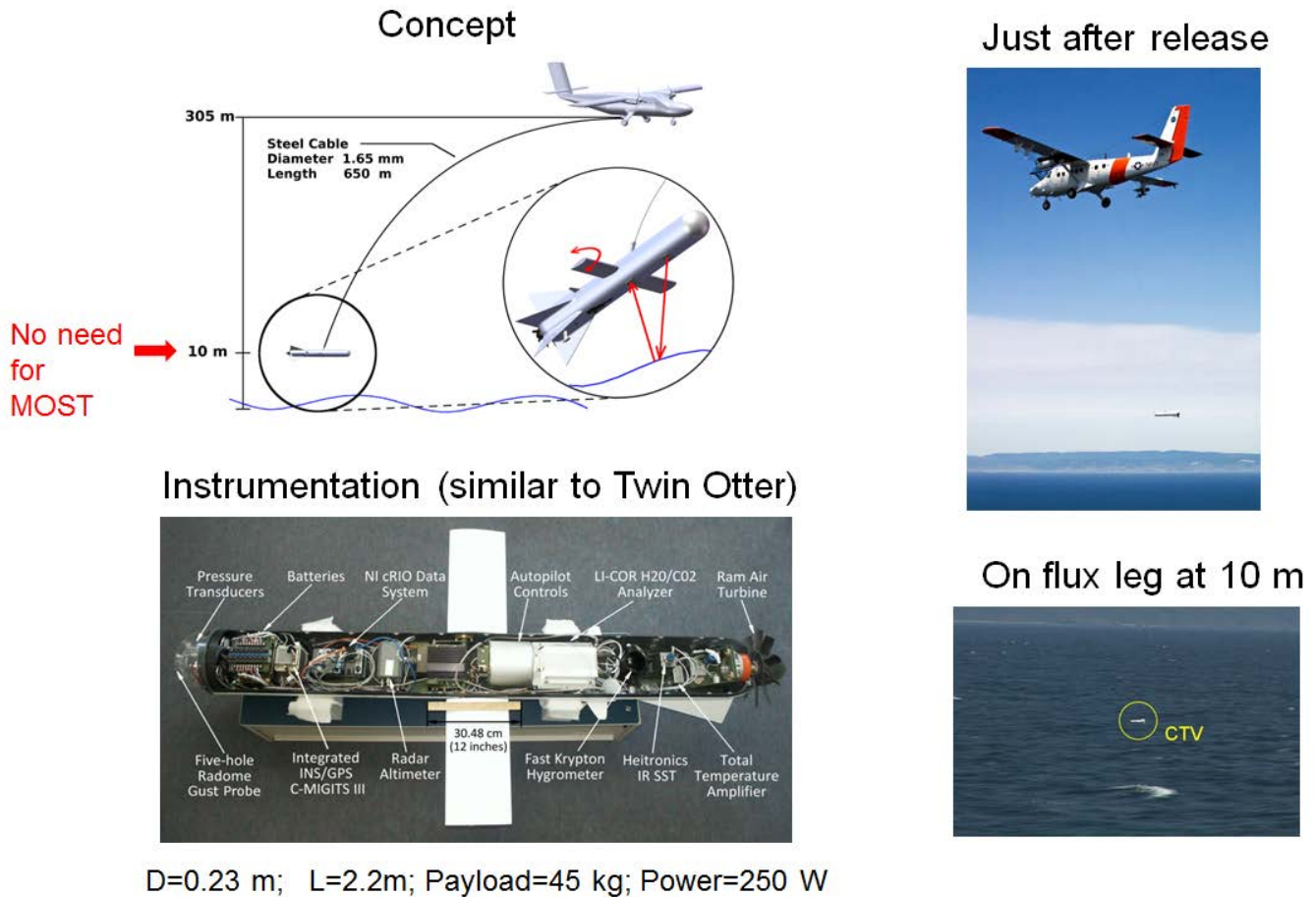


Figure 11. From top and clockwise: Controlled Towed Vehicle (CTV) height-keeping concept; CTV just after release from TO and being reeled out; CTV on flux run at 10 m off Pt Sur; CTV instrumentation.

Prior to UPPEF, extensive analyses of CTV flights showed that the vertical wind speed contamination by the CTV pitching oscillation was due to the original Meggitt control system being inadequate for the requirements of our application (April 2007 and April 2008) and to leaky pneumatics in the nose gust radome system in addition to a defective angle of attack pressure transducer (UPPEF test flight of July 27, 2012). These problems were corrected before UPPEF. During UPPEF, the CTV was grounded for many days to trouble-shoot problems caused by some undesired modifications that were made to the original (we had back in 2007 and 2008) data system and noisy nose video RF link that allows the flight crew and the CTV operator to detect small vessels that might be ahead of the CTV. In order to safely operate the CTV at 10 m or so, it is required to have a good enough quality video

from the CTV forward-looking nose camera displayed real-time at the flight deck and at the CTV control station. While the data system became operational by September 18, 2012, the video communication remained problematic throughout UPPEF and the CTV could not be operated below 17 m. The CTV was flown on 6 UPPEF flights (refer to Table 1) and on few shorter flights during the same period that were dedicated to CTV testing. During the 4 last flights, it performed very well albeit it could not be operated at 10 m. Data from the CTV were all processed and the analysis so far has focused on assessing the performance of new CTV control system and detecting OLEs especially the 30Sep2012 morning when the TODWL .

Most of the UPPEF flights were in low to moderate winds conditions with very little wave breaking and hence very little spray to be an issue for AGL laser altimeter used in the control system. There were short lived problems due to very low clouds but in general, performance of the AGL was good.

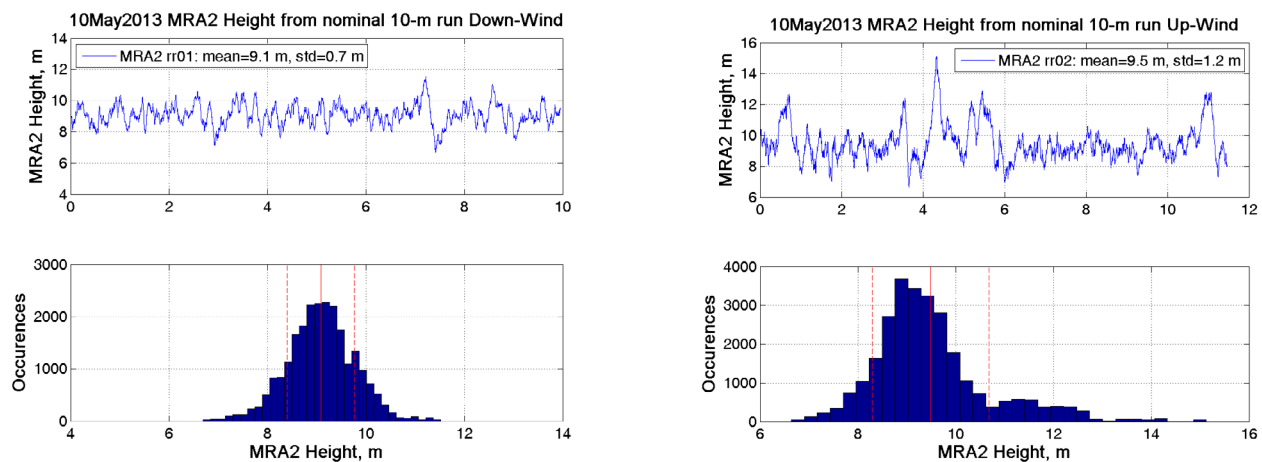


Figure 12. CTV elevation (top) and histogram (bottom) from MRA2 radar altimeter at a nominal 10-m controlled down-wind (left) and up-wind (right) runs. Altitude mean and standard deviation are given in the insert (top) and shown as solid (mean) and dashed ($\pm\sigma$) red lines (bottom). The CTV height-keeping performed remarkably well at just over 9 m with only 0.7 m standard deviation down-wind and at 9.5 m with 1.2 m standard deviation up-wind.

In order to have a more reliable all weather control system, we decided to replace the laser AGL sensor by the highly accurate Roke Miniature Radar Altimeter Type 2 (MRA2) owned by UCI after making sure the MRA2 performed very well during extensive testing on the Twin Otter during UPPEF. After UPPEF, a great deal of effort was made to integrate the data stream from the MRA2 into the CTV Piccolo autopilot processor and to extensively ground-test the Piccolo/MRA2 control system. On May 10, 2013, we conducted a test flight of the CTV with this new control configuration. The height-keeping performance down to ~ 9 m was very good even in relatively high winds ($\sim 15 \text{ m s}^{-1}$) and significant wave breaking for reciprocal (down-wind/up-wind) runs with a total duration over 21 minutes as shown in Fig. 12. The CTV mean radar height was 9.1 m with only 0.7 m standard deviation in the down-wind leg and 9.5 m with 1.2 m standard deviation in the up-wind leg. Albeit occasional excursions to higher elevations during the up-wind leg, the performance is much better than that of the aircraft at 30 m.

The means and standard deviations of the CTV MRA2 elevation from all 19 straight and level runs ranging from ~9 m to ~92 m are shown in Fig. 13. Compared to the higher altitude runs, the lowest runs (~10 m) have a slightly larger standard deviation but it is still very small (less than 1.4 m) considering the high wind and associated waves conditions. The data clearly show that the Piccolo/MRA2 height-keeping system worked very well over the broad range of altitudes. As further evidence of the CTV flight stability and robustness, similar plots for the CTV pitch and roll angles are shown in Fig. 14. The CTV pitches down 3° more at the lowest runs compared to higher ones. This results from the control wing being at its maximum downward orientation of -12° to overcome the lift from the tow cable and maintain the CTV down low. The pitch angle standard deviation, however, remains small ($\sim 0.7^\circ$) and is about the same for all runs. This is a crucial and an important improvement compared to the original (2007/2008) Meggitt control system that induced very large amplitude and pitching oscillation that contaminated the wind vertical component signal. The roll angle is very small and essentially remains within $\pm 0.5^\circ$.

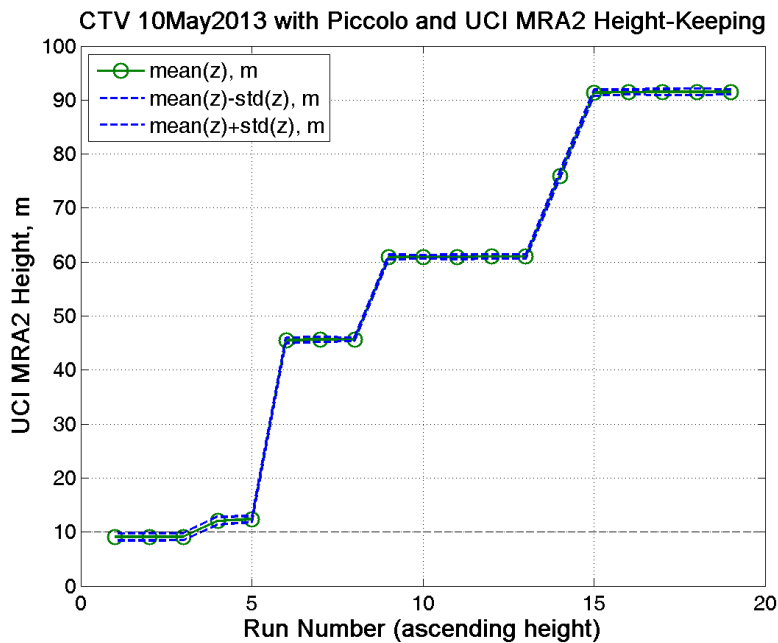


Figure 13: CTV radar altitude from MRA2, z , for all 19 straight and level runs on May 10, 2013: means (green circles and line), $\pm 1 \sigma$ (blue dashed lines). The runs are sorted and numbered from lowest to highest altitudes. Compared to the higher altitude runs, the lowest runs (~10 m) have slightly larger standard deviation but it was still very small (less than 1.4 m) considering the high wind and associated waves conditions. The data clearly show that the Piccolo/MRA2 height-keeping system worked very well even slightly below 10-m.

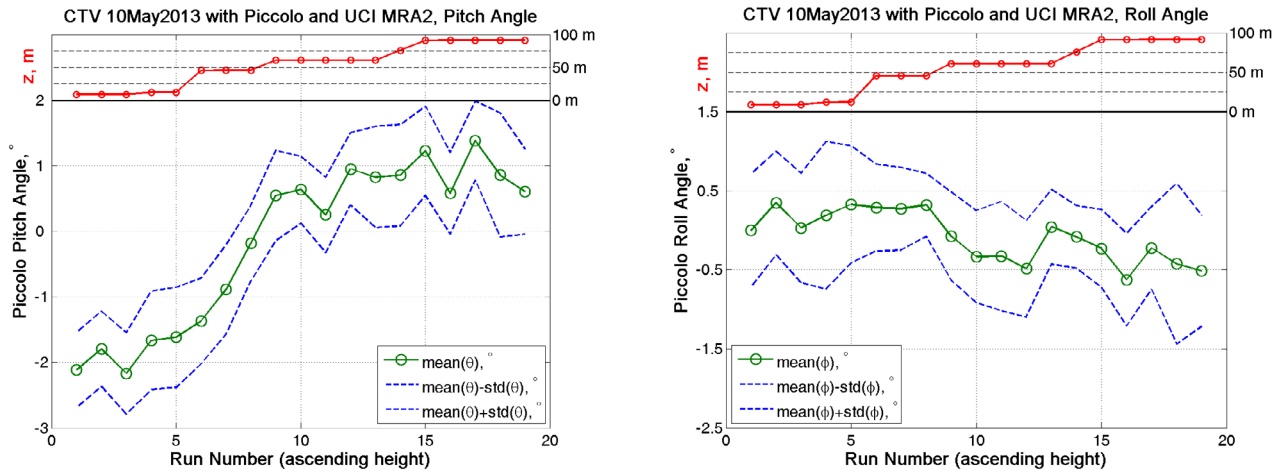


Figure 14: CTV Pitch angle, θ , (left) and roll angle (right) from Piccolo autopilot for all 19 straight and level runs: means (green circles and line), $\pm 1 \sigma$ (blue dashed lines). The runs are sorted and numbered from lowest to highest altitudes. The top red line and circles represent the MRA2 run means with their associated axis on the top left. The CTV pitches down 3° more at the lowest runs but the pitch angle standard deviation remains small (0.7°) and is about the same for all runs. This is a crucial and a huge improvement compared to the original (2007/2008) Meggitt control system. The roll angle is very small and remains within $\pm 0.5^\circ$.

The power spectra densities of vertical component of the wind from CTV runs on 15Apr2007 (original Meggitt control system), 27Jul2012 (AGL laser altimeter and Piccolo autopilot with leaks in radome wind system), 18Sep2012 (AGL laser altimeter and Piccolo autopilot but with “loose” control settings) and finally for 10May2013 (UCI MRA type 2 altimeter and Piccolo autopilot) are shown in Fig. 15. The spectra for 18Sep2012 and 10May2013 no longer exhibit the 0.8-Hz spurious large peak characteristic of the original Meggitt control system (15Apr2007) nor the less energetic 1-Hz peak (27Jul2012) that was attributed to faulty angle of attack transducer and leaks in the radome pressure lines. The wind vertical component is no longer affected by the CTV pitching oscillation whose standard deviation did not exceed 0.62° during the ~ 10 -m runs.

One thing of note that was observed and was common to the lowest level runs ($z < 14.5$ m) on the flight of 10May2013, is that after 2-Hz or so, the vertical wind speed spectra follow a $-4/3$ slope rather than the $-5/3$ slope characteristic of the inertial subrange in isentropic turbulence. A possible explanation could be technical: the motion data from the Piccolo used as an alternate are not as good as those of the C-MIGITS which were not usable (due to the start without GPS signal). This does not explain though why it is observed only on the lowest runs. It could also be physical as turbulence statistics are modified by ocean surface waves-induced motion this close to the surface. This was corroborated by recent results by Peter Sullivan from NCAR (shown at the ONR peer-review meeting) he obtained from very high resolution LES model in very similar wind and sampling conditions. Also

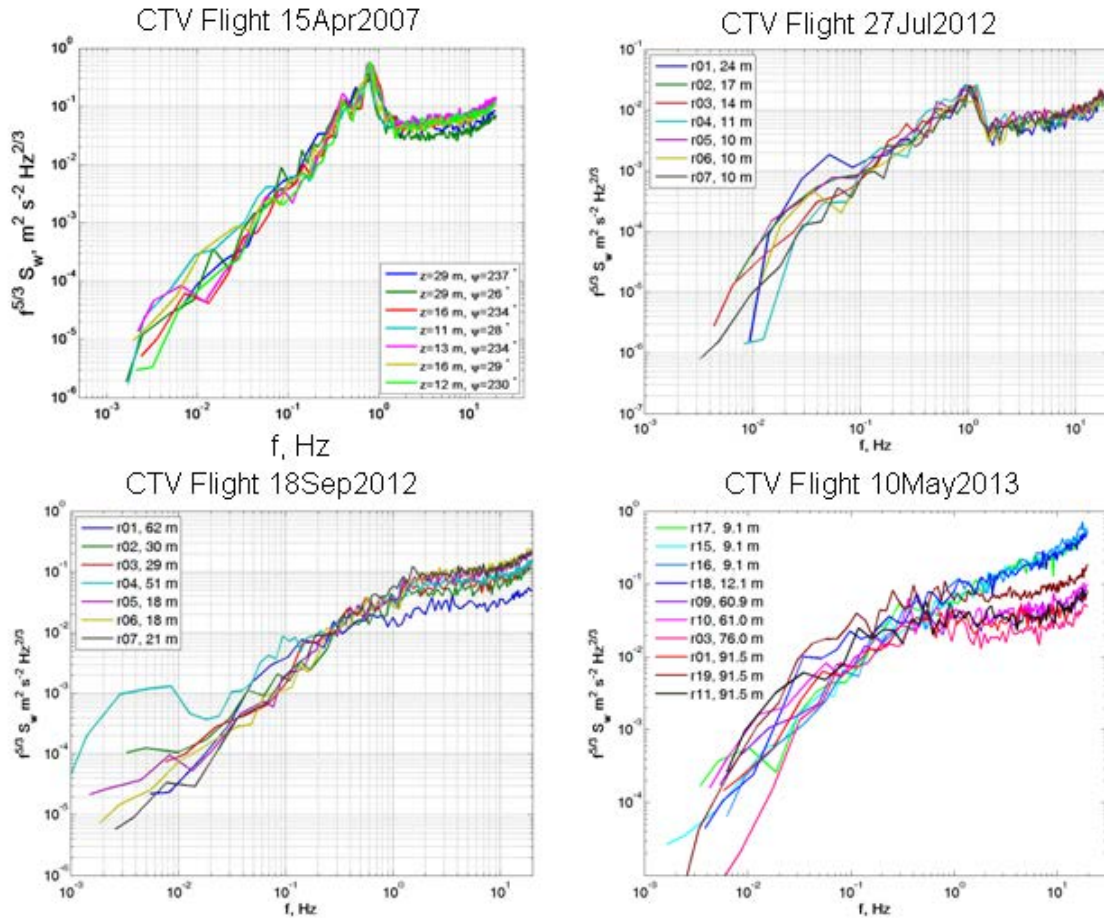


Figure 15: Power spectral densities times frequency^{5/3} of the wind vertical component obtained from CTV flights on 15Apr2007 (top, left), 27Jul2012 (top, right), 18Sep2012 (bottom, left), and on 10May2013 (bottom, right). The spectra for 18Sep2012 and 10May2013 no longer exhibit the 0.8-Hz spurious large peak characteristic of the original Meggitt control system (15Apr2007) nor the less energetic 1-Hz peak (27Jul2012) that was attributed to faulty angle of attack transducer and leaks in the radome pressure lines. The -5/3 inertial subrange is resolved up to ~10 Hz for 18Sep2012 and 10May2013 except for the lowest runs on 10May2013 that seem to follow a -4/3 slope. It should be noted that due up-wind and down-wind tracks were flown on 10May2013 instead of the usual cross-wind

these flux runs included some slight turns to remain within the cloud-free area as much as possible and to stay at as safe distant from the curvy coast line. These runs were flown roughly on an upwind and downwind track (due to the narrowness of the clear area) instead of the usual crosswind tracks which is most effective for correctly sampling the roll vortices which are roughly aligned with wind direction. The presence of such rolls was also one of the features shown by Peter Sullivan. Furthermore, our own results obtained from analysis of the UCI Met Mast measurements on the stable R/V FLIP during HiRes showed atypical stress divergence in similar conditions in the lowest ~15 meters when the waves phase speed was greater or of the order of the wind speed .

This question of the slope of the vertical wind speed spectra in itself is worth being investigated further, as to our knowledge, this is the first time turbulence data are obtained at ~10 m with an essentially non-intrusive platform (the CTV) compared to ships and buoys whose measurements are notoriously prone to flow distortions and to motion contamination.

A lingering issue with the CTV has been the real-time transmission of the analog video signal from its nose forward-looking camera to the flight deck and operator on the Twin Otter tow aircraft. The live video is not required by the active height-keeping control system on the CTV but it is rather a safety requirement so that the pilots and operator on the TO can spot any small vessels ahead of the CTV that are not detected by the aircraft nose radar or seen by the pilots. In early September 2014, we performed extensive ground tests at CIRPAS on the existing video transmitter/receiver pairs to characterize the shortcomings (range, image quality, interference with other communication systems) of each one of them. This helped us determine the specifications of the optimal transmitter/receiver pair. Subsequently, we obtained from a leading manufacturer demo units that would meet these specifications. Ground tests of the demo pair were very conclusive and confirmed it provides very good quality picture, has plenty of range and does not interfere with the two other CTV communication links (science data and CTV control) or with the GPS L1, L2 signals. This is a significant progress and there should be no technical limiting factor for routine operation of the CTV at 9-10 m over the ocean.

In our future work, once we get our year 3 funding, we plan to:

- Continue the cooperative work with the modeling group on the case study flight (31Aug2012) and identify another flight with more homogeneous conditions to test the sensitivity of the models
- Correct the IR SST measurements to account for reflected downwelling longwave radiation (i.e., reflected sky IR irradiance) using the work of Hignett, 1998 and Katsaros, 1980.
- Account for the absorption and emission of the underlying atmosphere (Burns et al. 2000). We expect the humidity correction to be small except perhaps for the higher level flux runs flown just below cloud base.
- Compare the eddy covariance fluxes to bulk fluxes (using corrected SST) from the latest COARE algorithm and Andreas & Mahrt new formulation. Particular attention will be paid to the environmental conditions (steadiness, homogeneity, cloud fraction, etc...) in these comparisons.
- Characterize the scale-dependence of the air-sea fluxes will be investigated using different averaging time periods on the long flux runs. This will be done with the sliding window method and the FFT-based ogive method.
- Characterize contributions to the fluxes from organized large eddies (OLEs) in cooperation with David Emmitt's group and Ralph Foster using the data from the 30Sep2012 morning flight when the TO Wind Doppler Lidar (TODWL) was functional.

We have made the UCI data and products from this project available on our web server. Summary plots from each flight can be found at: http://wave.eng.uci.edu/files/UPPEF/flights_plots/

3D plots with contoured potential temperature and dew point temperature (as in Fig. 2) for all 12 flights can be found at:

http://wave.eng.uci.edu/files/UPPEF/flights_plots/Soundings_3D_col/

High bandwidth (40-Hz) Twin Otter data and running averaging (180-s sliding window) fluxes from all straight and level runs in all 12 flights can be found at these password-protected URLs:

<http://wave.eng.uci.edu/files/UPPEF/datacuts/TO/>

<http://wave.eng.uci.edu/files/UPPEF/datacuts/TO/Fluxes/>

IMPACT/APPLICATIONS

The use of the LI-COR 7200 with our modified Rosemount total temperature probe housing used as inlet was successful. It provided reliable and fast response humidity measurements. Our modified krypton hygrometer is a good alternative to the obsolete AIR Lyman-alpha for fast-response humidity measurements from research aircraft.

The CTV height-keeping performance with the new control system we implemented is extremely good even at ~ 9 m above the surface in moderate to strong winds with significant waves breaking and sea spray. The CTV turbulence measurements and in particular the vertical component is of very good quality. Now that the last remaining issue of insufficient range of the video link has been resolved, the CTV is platform fully ready for service.

TRANSITIONS

With the major improvements we made to the CTV control, instruments and safety, this platform is ready for use in air-sea interaction research projects. In fact, we will be using it in the Coupled Air-Sea Interaction and EM Ducting Research (CASPER) MURI project lead by Dr. Qing Wang of NPS. Its first IOP experiment is scheduled for October 2015 off Duck, NC.

RELATED PROJECTS

Coupled Air-Sea Interaction and EM Ducting Research (CASPER).

PUBLICATIONS

Petters, J. L., H. Jiang, G. Feingold, D. L. Rossiter, D. Khelif, L. C. Sloan, and P. Y. Chuang, 2013: A comparative study of the response of modeled non-drizzling stratocumulus to meteorological and aerosol perturbations. *Atmos. Chem. Phys.*, 13, 2507-2529, doi:10.5194/acp-13-2507-2013, 2013.

Kumala, W., K. E. Haman, M. K. Kopec, D. Khelif, and S. P. Malinowski, 2013: Modified Ultrafast Thermometer UFT-M and temperature measurements during Physics of Stratocumulus Top (POST). *Atmos. Meas. Tech.*, 6, 2043-2054, doi:10.5194/amt-6-2043-2013, 2013.

Gerber H., G. Frick, S. P. Malinowski, H. Jonsson, D. Khelif and S. Krueger, 2013: Entrainment rates and microphysics in POST stratocumulus. *J. Geophys. Res. Atmos.*, 118, 12,094-12,109, doi:10.1002/jgrd.50878.

Malinowski, S. P., H. Gerber, I. Jen-LaPlante, M. K. Kopec, W. Kumala, K. Nurowska, P. Y. Chuang, D. Khelif, and K. E. Haman, 2013: Physics of Stratocumulus Top (POST): turbulent mixing

across capping inversion. *Atmos. Chem. Phys.*, 11, 12171-12186, doi:10.5194/acp-13-12171-2013, 2013.

Carman, J. K., D. L. Rossiter, D. Khelif, H. H. Jonsson, I. C. Faloona, and P. Y. Chuang, 2012: Observational constraints on entrainment and the entrainment interface layer in stratocumulus. *Atmos. Chem. Phys.*, 12, 11135-11152, doi:10.5194/acp-12-11135-2012, 2012.

Mahrt, L., D. Vickers, E. Andreas, and D. Khelif, 2012: Sensible Heat Flux in Near-neutral Conditions over the Sea. *J. Phys. Oceanogr.*, 42, 1134-1142. doi:10.1175/JPO-D-11-0186.1

Mahrt, L., and D. Khelif, 2010: Heat fluxes over weak SST heterogeneity, *J. Geophys. Res.* 115, D11103, doi:10.1029/2009JD013161.

Khelif, D., C. A. Friehe, H. Jonsson, Q. Wang, and J. Kalogiros, 2005: Wintertime Boundary-Layer Structure and Air-Sea Interaction over the Japan/East Sea. *Deep Sea Research*, 52, 1525-1546.